COMMUNICATION

Finned hierarchical MOFs supported on cellulose for the selective adsorption of n-hexane and 1-hexene

Received 00th January 20xx, Accepted 00th January 20xx

DOI: 10.1039/x0xx00000x

Xinyang Yin, a Jie Zha, a Skyler Gregor, abt Shengzhe Ding, a Ahmad Alsuwaidi, and Xueyi Zhang at

Finned hierarchical MOF particles (Cu(BDC) nanosheets as fins grown perpendicularly on Ni₂(BDC)₂(DABCO) hexagonal prisms) were synthesized on mofidied cellulose support. The hierarchical MOF particles exposed the open Cu(II) sites on Cu(BDC) to enable selective 1-hexene/n-hexane separation.

Alkenes are commodity chemicals that can be used as feedstocks to produce plastics, fuel additives and rubber, and one type of typical impurity in alkenes are their corresponding isoskeletal alkanes.[1,2] Alkane/alkene separation has been challenging due to their very similar physical properties, such as similar boiling points and similar kinetic diameters.[3] Even though such separations can be achieved using conventional distillation or membrane processes, the energy consumption to achieve such separations in large-scale is immense. [4-6] Separation methods exploiting their differences in chemical properties have the potential of achieving higher selectivity without increasing the energy consumption. Previously, porous adsorbents containing precious metal [7-10] as well as pure metal-organic frameworks (MOFs) $^{[11-13]}$ have been shown to yield high alkane/alkene selectivity due to favourable adsorption of C=C double bonds on the metal components. These adsorbents showed excellent capacity and selectivity in the separation of gaseous alkanes/alkenes. In order to achieve the separation of liquid hydrocarbons, extra considerations need to be taken regarding the slower mass transfer stemming from the stronger attractive interactions between molecules in liquids, as well as the accessibility of the larger hydrocarbons to adsorption sites. Therefore, a straightforward method to enhance liquid mass transfer would be to incorporate mesopores and to increase available adsorption sites per unit

Figure 1. Cellulose properties and surface modification: a). schematics of porous fibril network of commercial cellulose acetate membrane; b). 200 nm pores and fibril network of commercial cellulose acetate membrane shown in SEM; c). surface modification process: APTES ((3-aminopropyl)triethoxysilane) was used to convert -OH to -NH₂, where -NH₂ can provide coordination sites for attaching metal for subsequent MOF growth.

mass of adsorbent. We have previously shown that 2-D MOF

particles can increase adsorption capacity and selectivity from liquid phase. $^{[14,15]}$ We have also shown that pillared MOFs with aromatic rings can increase the adsorption of alkenes over alkanes. $^{[16]}$ In this study, we combined morphology control methods utilized in our previous studies, and introduced cellulose-supported hierarchical MOF coatings to the separation of n-hexane and 1-hexene. Hierarchical MOF (Cu(BDC) grown on $Ni_2(BDC)_2(DABCO)$, BDC=1,4-benzenedicarboxylate (terephthalate), DABCO=1,4-diazabicyclo[2.2.2]octane) was grown on surface-modified

cellulose, and the calculated adsorptive selectivity of 1-hexene

Electronic Supplementary Information (ESI) available: [details of any supplementary information available should be included here]. See DOI: 10.1039/x0xx00000x

Cellulose

^a Department of Chemical Engineering, The Pennsylvania State University, University Park, PA 16801.

b. Chemical Engineering Program, Century College, White Bear Lake, MN 55110.

[†] Current Address: Department of Chemical Engineering and Materials Science, University of Minnesota, Minneapolis, MN 55455

^{*} Corresponding author: xuz32@psu.edu

COMMUNICATION Journal Name

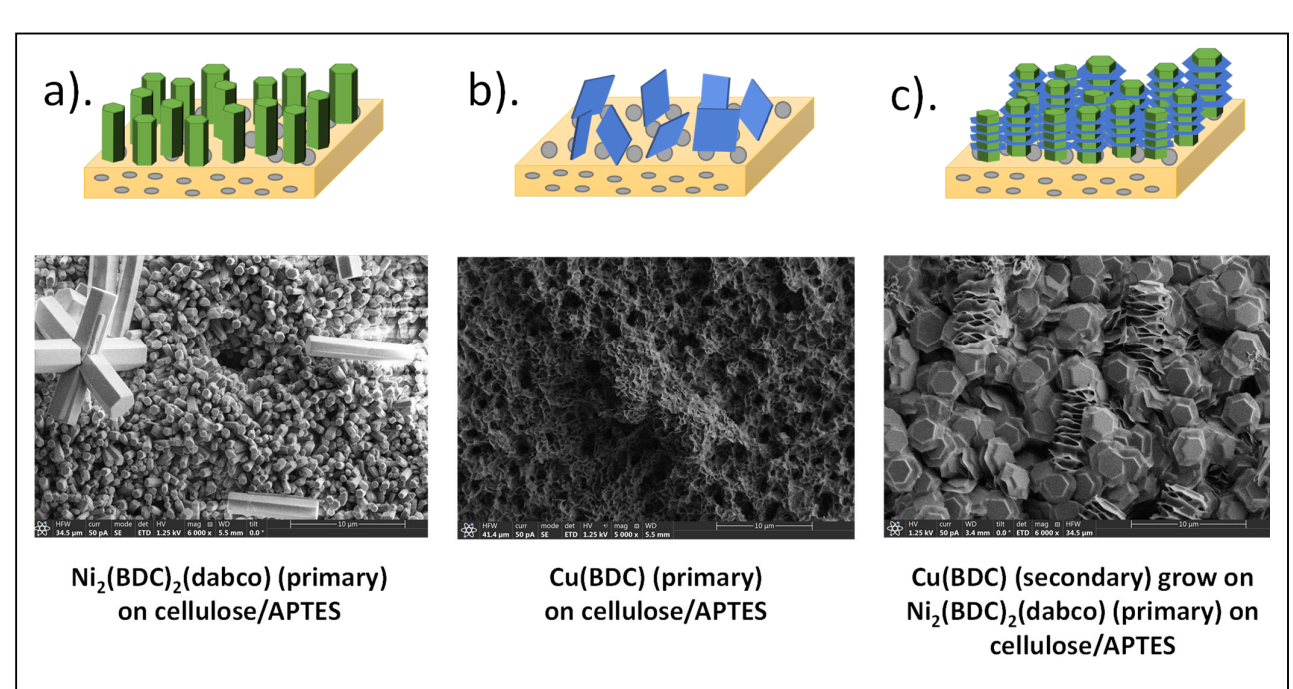


Figure 2. MOF morphology and orientation on Cellulose/APTES: a). Ni₂(BDC)₂(dabco) grown on APTES-modified cellulose support, where rod-shapes MOF particles are primarily grown perpendicularly to the support; b). Cu(BDC) grown on APTES-modified cellulose support, where randomly-oriented 2-D MOF particles are grown perpendicularly on the support; c. Cu(BDC) (nanosheets, secondary particle) grown on Ni₂(BDC)₂(dabco) (rods, primary particle), where the large surfaces of the nanosheets are exposed and additional mesopores are present between Cu(BDC) "fins".

and 1-hexane was 11.4, which is higher than previously reported data from Co/Mg-MOF- $74^{[17]}$ and other porous materials $^{[18-21]}$ (Table S1).

The cellulose used in this work was hydrolyzed from commercial cellulose acetate membranes, based on a previously reported method ^[14, 22]. (Figure 1, detailed experimental procedure in ESI) The pores of cellulose acetate were approximately 200 nm in size, and the pore size remained the same after hydrolysis (as shown in the SEM image in Figure 1.b). The 200 nm pore size was suitable for MOF attachment at the same time not too small to impede the diffusion of large guest molecules.

Subsequent surface functionalization of cellulose was necessary to attach MOFs with controlled orientation and practical particle density. According to our previous report^[15], the surface functional group determines the density of MOF particles attached and its orientation on cellulose. It was found that -OH groups on cellulose surface could not attach MOF particles with high density.^[15] Also, -OH groups will result in random orientation of MOF particles attached to cellulose. For the purpose of liquid-phase separation, the random orientation of MOF could lead to reduced surface area and consequentially reduced adsorption amount. Therefore, APTES was used to convert the surface -OH to -NH₂ (Figure 1.c).

We chose pillared MOF $Ni_2(BDC)_2(DABCO)$ as primary MOF on cellulose/APTES because the Ni MOF has an elongated hexagonal prism shape, providing large surface area for

attaching secondary MOFs ("fins") on the sides. The elongated morphology resulted from the anisotropic structure of pillared MOFs, because the two linkers (BDC and DABCO) coordinate with Ni at different rates. In our case, Ni coordinates with BDC in the equatorial plane slower and resulted in small base faces. The DABCO coordinate with Ni faster in the axial direction which connects the equatorial planes. As a result, the axial direction is the largest dimension in this $Ni_2(BDC)_2(DABCO)$ hexagonal prism. When the smaller hexagonal prism base faces coordinated with -NH $_2$ and attached on cellulose/APTES, the $Ni_2(BDC)_2(DABCO)$ exposed its largest surface, the 6 sides, for attaching Cu(BDC) nanosheets (Figure 2. a).

Cu(BDC) is a MOF with unsaturated Cu(II) sites, suitable for selective adsorption of alkenes over alkanes. It has 2D sheet morphology with high aspect ratio which leads to larger surface area for alkene/alkane separation. Inspired by our previous report[15], seeded growth method could produce secondary heterometallic MOFs with larger external surface area compared to primary MOFs, thanks to the preservation of interparticle mesopores. Cu(BDC) nanosheets were grown on the Ni₂(BDC)₂(DABCO) hexagonal prisms using seeded growth method. The Cu(BDC) nanosheets were perpendicularly and epitaxially attached as "fins" around the sides of hexagonal Ni MOF (Figure. 2c), exposing their unsaturated Cu(II) sites for alkene/alkane separation. The growth of Cu(BDC) on Ni₂(BDC)₂(DABCO) was because the two MOFs had no lattice mismatch at the interface. The specific relative orientation between the Cu(BDC) and Ni₂(BDC)₂(DABCO) particles indicates

Journal Name COMMUNICATION

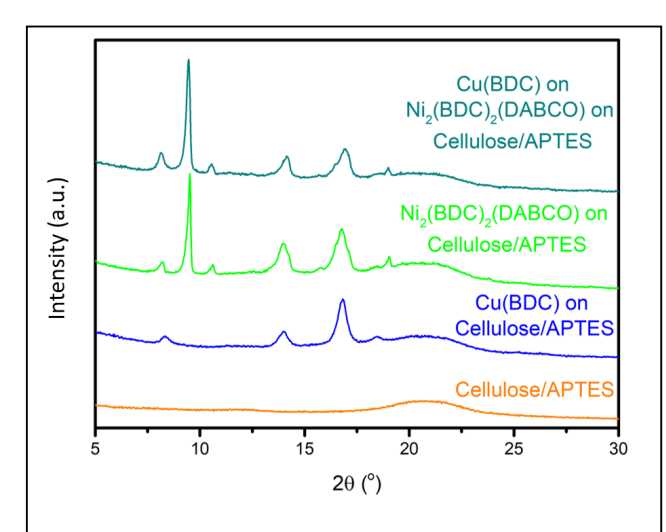


Figure 3. XRD patterns of the cellulose support and MOFs supported on cellulose. Bare APTES-modified cellulose support showed a broad peak around 21°. Cu(BDC) showed characteristic peak at 8°. Ni₂(BDC)₂(DABCO) showed characteristic peaks at 8° and 9°. The intergrown Cu(BDC) on Ni₂(BDC)₂(DABCO) did not show additional peaks, indicating that there was no other phases formed during intergrowth.

that the sample was an intergrowth, instead of a mechanical mixture of the two MOFs. Elemental analysis (Table S2) showed a Ni:Cu molar ratio of 2.6, supporting the presence of Cu MOF in the sample.

X-ray diffraction (XRD) was used to verify the crystallinity of the MOFs. The XRD patterns of MOFs supported on cellulose/APTES showed no other crystal structures, other than the intended MOF(s) (Figure 3). The cellulose/APTES by itself showed a characteristic broad peak around 21°, which is not overlapping with any peaks from the MOFs. Cu(BDC) showed characteristic peak at 8°, while Ni₂(BDC)₂(DABCO) showed characteristic peaks at 8° and 9°. The intergrown Cu(BDC) on Ni₂(BDC)₂(DABCO) did not show extra peaks, indicating that there was no other phases formed during intergrowth. The presence of characteristic structural features of the hierarchical MOF was also supplemented by IR spectroscopy (Figure S2). The presence of microporosity was confirmed with CO₂ physical adsorption (Figure S3).

The higher surface area and the exposed open Cu(II) sites synergistically improved the adsorption selectivity of 1-hexene. This is as expected from the design of this material and was confirmed by ¹³C NMR and IR (Figure S4 and S5). Four samples, bare cellulose/APTES support, Ni₂(BDC)₂(DABCO) grown on cellulose/APTES, Cu(BDC) grown on cellulose/APTES, and Cu(BDC)-on-Ni₂(BDC)₂(DABCO) grown on cellulose/APTES (the finned hierarchical MOF) were tested for n-hexane batch adsorption and 1-hexene batch adsorption. In both experiments, cyclohexane was used as solvent for n-hexane and 1-hexene, as employed by Sun *et al.* in a similar study.^[917] The adsorption amount and selectivity between n-hexane and 1-

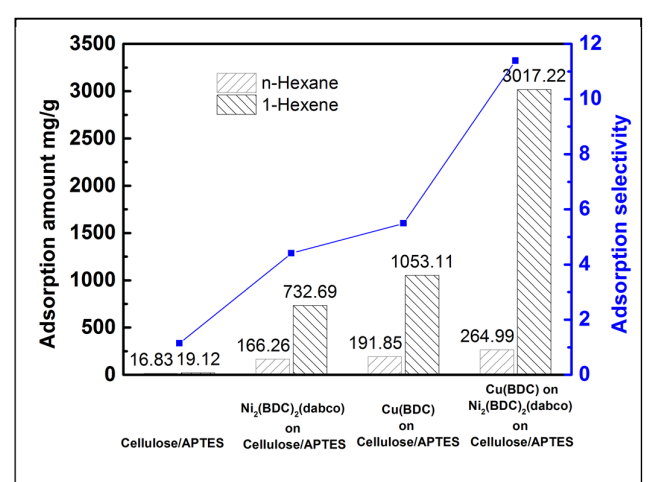


Figure 4. Batch adsorption amount and calculated selectivity of 1-hexene and n-hexane on bare APTES-modified cellulose, Ni₂(BDC)₂(DABCO) grown on cellulose/APTES, Cu(BDC) grown on cellulose/APTES, and Cu(BDC)-on-Ni₂(BDC)₂(DABCO) grown on cellulose/APTES (the finned hierarchical MOF). Experimental details are in ESI.

hexene for each sample were shown in Figure 4. Cellulose/APTES barely adsorbed n-hexane or 1-hexene, which is expected due to the lack of strong interactions between hydrocarbons and surface -OH and -NH2 groups. The individual MOFs (Ni₂(BDC)₂(DABCO) and Cu(BDC)) supported on cellulose/APTES both demonstrated larger adsorption amounts of n-hexane and 1-hexene. They also showed moderate calculated ideal selectivity between 1-hexene over n-hexane, which is between 4-5. This can be attributed to the intrinsic chemical properties of respective MOFs: the aromatic rings on pillared MOF could preferably adsorb alkenes due to π - π interaction with C=C double bonds, [16] and the Cu(II) open sites on Cu(BDC) preferably adsorbs alkenes over alkanes. [23] Cu(BDC) supported on cellulose showed slightly higher adsorption amount and selectivity. The hierarchical Cu(BDC)-on-Ni₂(BDC)₂(DABCO) on cellulose/APTES showed the highest adsorption amounts and calculated 1-hexene/n-hexane selectivity among the four samples. The calculated ideal selectivity is 11.4 between 1-hexene and n-hexane, which is higher than either individual MOF. The calculated selectivity is also higher than that obtained on Co/Mg-MOF-74 (approximately 10 with Co:Mg=3:7).[17] We attribute this to the exposed surfaces of Cu(BDC) particles intergrown on the Ni₂(BDC)₂(DABCO) hexagonal prisms, where the surface and metal sites were exploited to the maximum extent for adsorption. The adsorption amounts of pure hydrocarbons in the liquid phase showed the same trend, where the adsorption amount of pure 1-hexene was one order of magnitude higher than that of n-hexane (Table S3). Column breakthrough experiment also confirmed the ability of the hierarchical MOF material to selectively adsorb 1-hexene over n-hexane (Figure

COMMUNICATION Journal Name

In this work, we have shown that a finned hierarchical MOF, Cu(BDC)-on-Ni₂(BDC)₂(DABCO) grown on cellulose/APTES, exhibited 1-hexene and n-hexane adsorptive selectivity of 11.4. The high calculated selectivity is believed to stem from the adsorption sites whose exposure was maximized by the hierarchical morphology. Although we used n-hexane and 1-hexene as examples in this work, we would like to point out that the potential of this material also lies in separating larger molecules encountered in the production of fine chemicals and pharmaceuticals, where the major difference between the molecules could only be one C=C vs. one C-C (such as the separation of cannabidiol (CBD) and cannabinol (CBN)).

We acknowledge the financial support from the 3M Non-Tenured Faculty Award. We thank the U.S. National Science Foundation (Award EEC-1950639) for supporting Skyler Gregor's visit to the Pennsylvania State University. We acknowledge Dr. William G. Van Der Sluys (Penn State Altoona) for the technical help and discussion on IR spectra. We acknowledge Dr. David S. Bell (Restek Corporation) for providing chromatography supplies and experimental insights for the column breakthrough experiments.

- 16 X. Yin, and X. Zhang. *Materials Chemistry Frontiers* **2020**, *4* (10), 3057-3062.
- 17 H. Sun, D. Ren, R. Kong, D. Wang, H. Jiang, J. Tan, D. Wu, S. Chen, and B. Shen. *Microporous and Mesoporous Materials*, **2019**, *284*, 151-160.
- 18 P. E. Eberly, C. N. Kimberlin. *Journal of Applies Chemistry*, **1967**, *17*, 44.
- 19 R. Yang, R. Gao, Y. Wang, Z. Qian, G. Luo. *Langmuir*, **2020**, 36, 8597.
- 20 A. J. Nuñez, L. N. Shear, N. Dahal, I. A. Ivarram J. Yoon, Y. K. Hwang, J. S. Chang, S. M. Humphrey. *Chemical Communications* 2011, 47, 11855.
- 21 J. Bentley, G. S. Foo, M. Rungta, N. Sangar, C. Sievers, D. S. Sholl, S. Nair. *Industrial and Engineering Chemistry Research* **2016**, *55*, 5043.
- 22 Y. Xin, Q. Xiong, Q. Bai, M. Miyamoto, C. Li, Y. Shen, and H. Uyama. *Carbohydr. Polym.* **2017**, 157, 429–437.
- 23 P. Chowdhury, S. Mekala, F. Dreisbach, and S. Gumma. *Microporous and Mesoporous Materials*, **2012**, *152*, 246-252.

Notes and references

- 1 R. B. Eldridge, *Industrial & Engineering Chemistry Research*, **1993**. 32. 2208.
- Z. R. Herm, E. D. Bloch, and J. R. Long. *Chemistry of Materials* 2014, 26, 323-338.
- D. S. Sholl, and R. P. Lively. *Nature News* **2016**, 532.7600, 435.
- 4 M. Galizia, W. S. Chi, Z. P. Smith, T. C. Merkel, R. W. Baker, B. D. Freeman. *Macromolecules* 2017, 50, 7809-7843.
- 5 M T. Ravanchi, T. Kaghazchi, and A. Kargari. *Desalination*, **2009**, 235, 199.
- 6 W. J. Koros, and R. Mahajan, *Journal of Membrane Science*, **2000**, 175(2), 181-196.
- 7 J. G. Min, K. C. Kemp, and S. B. Hong. Separation and Purification Technology 2020, 250, 117146.
- 8 Y. Wang, Z. Hu, Y. Cheng, and D. Zhao. *Industrial & Engineering Chemistry Research*, **2017**, *56*, 4508-4516.
- 9 H. I. Mahdi, and O. Muraza, Separation and Purification Technology, 2019, 221, 126-151.
- S. U. Rege, J. Padin, and R. T. Yang, AIChE Journal, 1998, 44(4), 799-809.
- 11 A. Luna-Triguero, J. M. Vicent-Luna, P. Gómez-Álvarez, and S. Calero. The Journal of Physical Chemistry C, 2017, 121(5), 3126-3132.
- 12 M. G. Plaza, A. M. Ribeiro, A. Ferreira, J. C. Santos, Y. K. Hwang, Y.-K. Seo, U.-H. Lee, J.-S. Chang, J. M. Loureiro, A. E. Rodrigues. *Microporous Mesoporous Mater.* **2012**, 153, 178.
- 13 E. D. Bloch, W. L. Queen, R. Krishna, J. M. Zadrozny, C. M. Brown, J. R. Long. *Science* **2012**, 335, 1606.
- 14 J. Zha, X. Yin, J. R. Baltzegar, and X. Zhang, *Langmuir*, **2019**, 35(40), 12908-12913.
- 15 X. Yin, S. Tang, Q. Yong, X. Zhang, and J. M. Catchmark. Separation and Purification Technology 2021, 119366.